

pubs.acs.org/EF Article

Investigation of Ethanol Conversion on H-ZSM-5 Zeolite by *in Situ* Solid-State NMR

Shu Zeng, Junjie Li, Nan Wang, Wenna Zhang, Yingxu Wei, Zhongmin Liu,* and Shutao Xu*



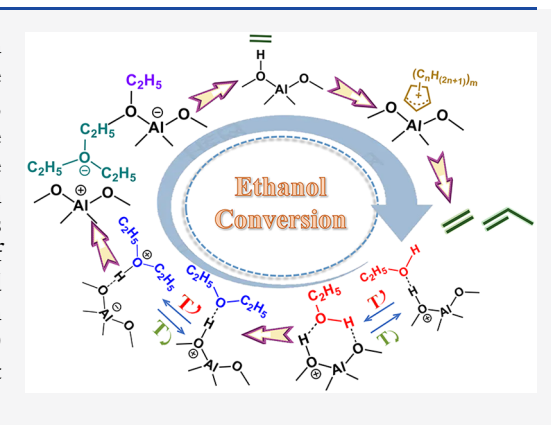
Cite This: Energy Fuels 2021, 35, 12319-12328



ACCESS



ABSTRACT: The process of ethanol conversion on H-ZSM-5 zeolite with different Si/Al ratios was well-studied with the assistance of *in situ* solid-state ¹³C NMR experiments under continuous flow (CF) and batch-like conditions, respectively. Except for the adsorbed ethanol and diethyl ether, the surface ethoxy species, triethyloxonium ion, and even cyclopentadienyl cations were captured on the working catalyst and identified as active intermediates in ethanol conversion. The evolution process of these captured intermediates was exhaustively illustrated subsequently. Especially, two kinds of configuration of the adsorbed ethanol, referred to as side-on and end-on orientations, and diethyl ether (DEE) with an activated state were also revealed in this work. In addition, involved as one of the important active intermediates in MTO reaction, the cyclopentadienyl cations were also speculated to play important roles in the ethanol conversion and have close relation to propene formation.



Article Recommendations

1. INTRODUCTION

With the rapid development of national economy, the demands for energy and fuel have become increasingly urgent. However, the continued depletion of fossil energy and stricter environmental policies urge the researchers to find a green and renewable energy resource to alleviate these situations. Bioethanol, derived from biomass, has become a befitting alternative in the energy market due to its renewable nature and low CO₂ emission. Except for the traditional sugar fermentation from sugar crops, ^{2,3} lignocellulose biomass like agricultural and forester residues also have tremendous potential in bioethanol production on a large-scale, ^{4,5} which makes it anticipated for conversion bioethanol to higher value-added chemicals.

Light olefins like ethene and propene are major chemical raw materials. For example, the polymerization of ethene can provide various polyethene products; the epoxidation of propene is another important industrial process for epoxypropane and acrylic acid. Although great progress has been made in coal-to-olefin technology like methanol-to-olefin (MTO), ^{6,7} the major source of light olefin primarily relies on an oil resource. The increasing demands for light olefins in the industrial field drive researchers to turn their attention to renewable feedstocks. Ethanol conversion to olefins like ethene and propene provides a bridge between petrochemical industry and renewable biomass and has attracted considerable attention from both academia⁸ and industry.⁹

Among of the various heterogeneous catalysts, zeolites have uniform pore structure, high surface area as well as adjustable acidity, which makes it a popular catalyst in ethanol conversion reaction, especially ZSM-5 zeolite. 10,11 Many published works have been done to investigate the details in ethanol conversion, including the reaction temperature, 12,13 contact time, 14,15 and Si/Al ratios 16,17 of used zeolites. It was concluded that a high temperature and long contact time favors the formation of the long chain olefins. In addition to these factors, the Si/Al ratios also have a significant effect on products selectivity. It was found that the low Si/Al ratios of ZSM-5 zeolite, which means a high concentration of acid sites, would accelerate the ethanol conversion to form more long chain olefins and even the carbonaceous deposits on catalyst. 18 Although the reaction conditions have been systematically studied in ethanol conversion, the reaction mechanism and active intermediates, which is crucial for improving catalytic performance, remain unclear. Some active intermediates such as ethoxy^{19,20} was detected during the ethanol dehydration stage and is generally considered as the precursor to ethene. Zhou et al. also reported a triethyloxonium ion in the dehydration stage of ethanol, which provides an energetically favorable route to form ethoxy species and then produce ethene at a low temperature.²¹ In addition, some ethyl-substituted benzenes were demonstrated that have important roles in the formation of ethene analogous

Received: June 29, 2021 Revised: July 14, 2021 Published: July 23, 2021





to the polymethylbenzenes in methanol-to-olefins reaction.²² However, the detailed correlation between the active species still needs to be further explained. Furthermore, it is also imperative to capture the other active species except for the intermediates mentioned above.

In this work, the whole dehydration process of ethanol was clearly exhibited using in situ 13 C magic angle spinning nuclear magnetic resonance (MAS NMR) spectroscopy. Except for the adsorbed ethanol and diethyl ether, the surface ethoxy species, triethyloxonium ion, and even cyclopentadienyl cations were captured on the working catalyst and identified as active intermediates in ethanol conversion. The evolution of the captured intermediates was well-explained. In addition, the concentration of cyclopentadienyl cations that were confined in the zeolite framework decreased with the increase of the Si/ Al ratios of H-ZSM-5 zeolite, accompanied by a decline of the selectivity of propene. Involved as one of the important active intermediates in MTO reaction, the cyclopentadienyl cations were also proposed to have important roles in the ethanol conversion, and the concentrations of the captured cyclopentadienyl cations were speculated to have close relation to propene selectivity.

2. EXPERIMENTAL SECTION

2.1. H-ZSM-5 Zeolites Preparation. ZSM-5 zeolites with different Si/Al ratios used in this work were synthesized according to ref 23. The different Si/Al ratios of the ZSM-5 zeolite were obtained by varying the content of the $AlCl_3\cdot 6H_2O$ solution and ethylamine (C_2H_7N) aqueous solution (65 wt % in H_2O) in the gel. As shown in Table 1, the molar ratio of each component in the final

Table 1. Composition of Raw Materials for Synthesis of H-ZSM-5 Zeolite with Different Si/Al Ratios

sample	$Al_2O_3(y)$	$C_2H_7N(z)$	Si/Al ^a	Si/Al ^b
H-ZSM-5-26	0.02	0.27	26	26.6
H-ZSM-5-45	0.01	0.20	45	45.5
H-ZSM-5-150	0.0025	0.04	150	150.4
H-ZSM-5-351	0.001	0.04	351	350.9

 $^a\mathrm{Calculated}$ from XRF experiments. $^b\mathrm{Calculated}$ from $^{29}\mathrm{Si}$ MAS NMR spectra.

gel can be calculated as $SiO_2/Al_2O_3/TPABr/C_2H_7N/H_2O = 1:y:0.20:z:17$. The H-ZSM-5-x zeolites were obtained from the synthesized ZSM-5 zeolites, which were calcined at 600 °C for 6 h to remove the organic template, and x denotes the Si/Al ratio from X-ray fluorescence (XRF) analysis.

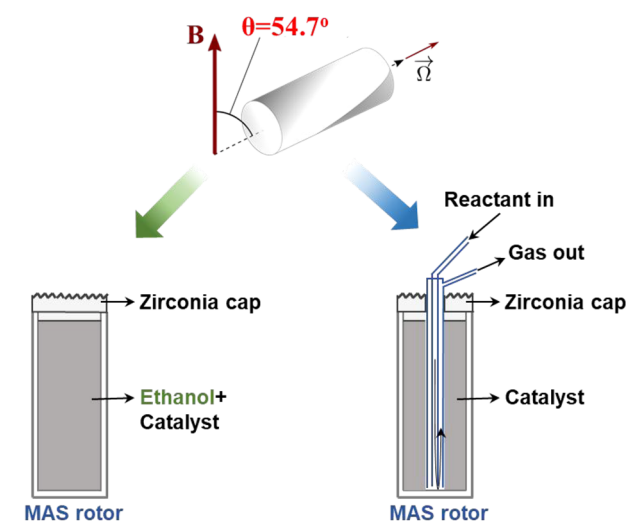
2.2. Catalyst Characterization. The powder X-ray diffraction (XRD) patterns were conducted on a PANalytical X'Pert PRO X-ray diffractometer with Cu K α radiation (λ = 1.54059 Å, 40 kV, 40 mA) to confirm the MFI structure of the synthesized catalysts. The crystal morphology was obtained using a Hitachi SU8020 field emission scanning electron microscope (SEM). An X-ray fluorescence (XRF) spectrometer (Philips Magix-601) was used to measure the chemical compositions of the samples. The N₂ adsorption—desorption experiments were performed to obtain more information about the pore structure at 77 K (Micromeritics ASAP 2020). Zeolites with different Si/Al ratios were pretreated at 673 K for 4 h under a vacuum. More detailed information about these experiments can refer to our reported work.²⁴

2.3. Solid-State NMR (ssNMR) Experiment. Solid-state NMR spectroscopy is a powerful technology on investigating the active species and local environment of the zeolite. ^{25,26} The ²⁹Si, ²⁷Al, and ¹³C MAS NMR experiments in this work were performed on a Bruker Avance III 600 spectrometer equipped with a 14.1 T wide-bore magnet. The resonance frequencies in this field strength are 119.2,

156.4, and 150.9 MHz for ²⁹Si, ²⁷Al, and ¹³C, respectively. The ²⁷Al MAS NMR spectra were recorded using a one pulse sequence with a 2 s recycle delay and $\pi/12$ pulse width of 0.7 μ s under a spinning rate of 12 kHz. The chemical shift of ²⁷Al NMR was referenced to l mol/L Al(NO₃)₃ solution at 0 ppm. The ²⁹Si MAS NMR spectra were recorded with a high-power proton decoupling sequence with a 10 s recycle delay and $\pi/2$ pulse width of 4.3 μ s under a spinning rate of 8 kHz. The chemical shift of ²⁹Si NMR was referenced to kaolinite at -91.5 ppm. Prior to the ¹H MAS NMR experiments, the samples were dehydrated with a home-built vacuum line at 420 °C for 18 h. The quantitative ¹H MAS NMR experiments were performed on a Bruker Avance III 500 spectrometer equipped with an 11.7 T widebore magnet. The resonance frequency in this field strength is 500.1 MHz for ¹H. The ¹H MAS NMR spectra were recorded using a one pulse sequence with a 150 s recycle delay, a 4 scanning number, and $\pi/2$ pulse width of 3 μ s under a spinning rate of 12 kHz. The Gaussian-Lorentz line was used in Dmfit software to deconvolve the spectra and then quantify the density of different acid sites. Adamantane was used as an external standard, and the chemical shift of ¹H was also referenced to adamantane at 1.74 ppm.

Here, two types of *in situ* ¹³C MAS NMR methods were used for studying the ¹³C-ethanol reaction (Scheme 1). One is under batch-

Scheme 1. Schematic Diagram of Two Types of in Situ ¹³C NMR Methods Consisting of the in Situ Batch-Like and in Situ Continuous Flow (CF) NMR Methods, Respectively



In situ batch-like NMR In situ CF NMR

like conditions and the other is under continuous flow (CF) conditions. Prior to the *in situ* ¹³C-ethanol reaction, the catalysts were dehydrated under the home-bult vacuum line at 420 °C overnight to remove the adsorbed water and impurities. In the *in situ* ¹³C MAS NMR experiment of ethanol conversion under batch-like conditions, about 20 kPa of ¹³CH₃. CH₂OH saturated vapor was adsorbed in the pretreated H-ZSM-5-26 zeolite at room temperature (RT), kept equilibrium for 30 min, and then evacuated for 1 min to remove the excess adsorbed ethanol from the sample surface. Subsequently, the samples with adsorbed ethanol were transferred into a 4 mm NMR rotor, which acted as a reactor in a nitrogen glovebox. The temperature-programmed ¹³C cross-polarization (CP) MAS NMR experiments were conducted using a 4 mm H-X probe with the temperature rising from 42 to 217 °C. The spinning rate was 10 kHz, and the recycle delay was 1 s.

In the *in situ* CF ¹³C MAS NMR experiment of ethanol reaction, about 0.2 g of pretreated H-ZSM-5-26 samples was filled into a 7 mm NMR rotor as a hollow cylinder in a nitrogen glovebox and then transferred into the 7 mm HX MAS-CAT probe. The catalysts were activated at 300 °C for 30 min *via* the heated bearing gas N₂, keeping

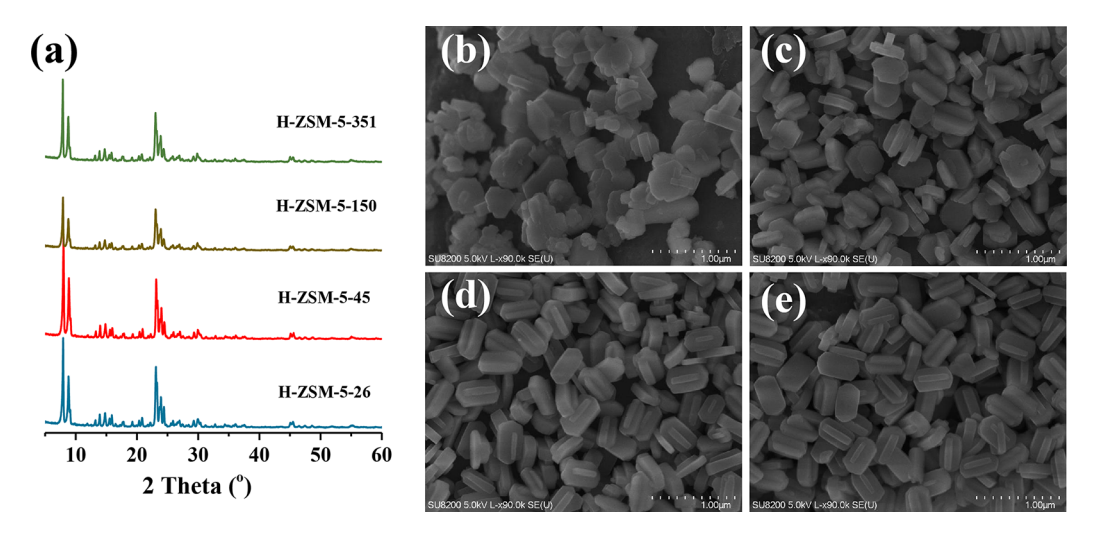


Figure 1. (a) XRD pattern and (b-e) the SEM of the synthesized H-ZSM-5 zeolite with different Si/Al ratios: (b) H-ZSM-5-26, (c) H-ZSM-5-45, (d) H-ZSM-5-150, and (e) H-ZSM-5-351.

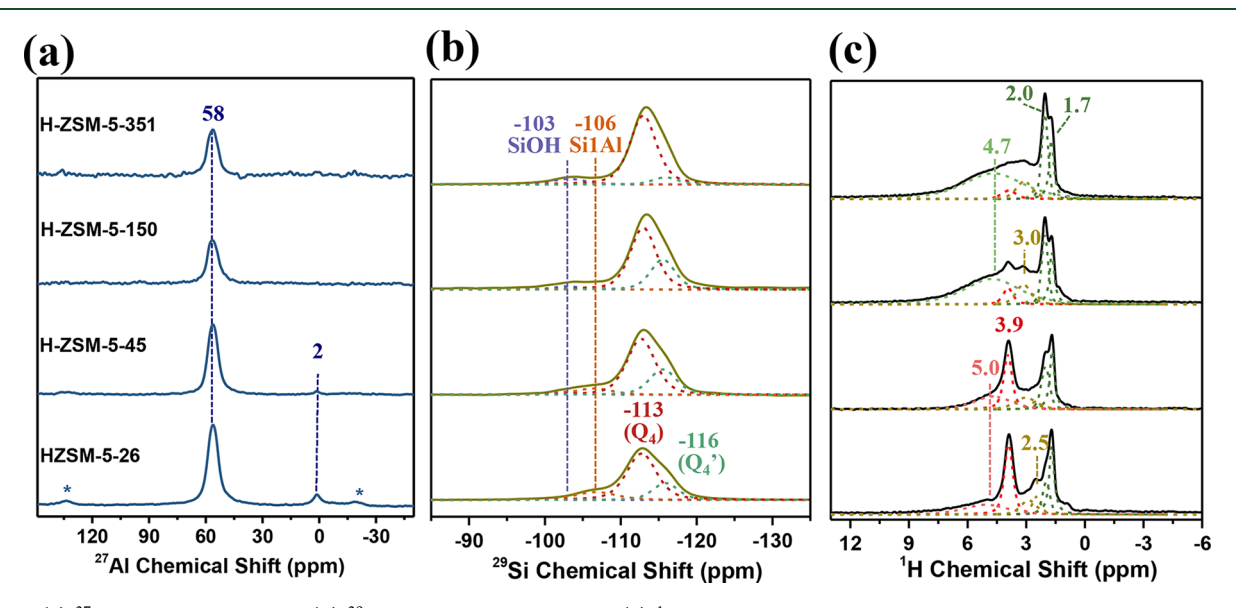


Figure 2. (a) ²⁷Al MAS NMR spectra, (b) ²⁹Si MAS NMR spectra, and (c) ¹H MAS NMR spectra as well as their corresponding deconvolution curves of the synthesized H-ZSM-5 zeolite with different Si/Al ratios.

the carrier gas helium injected into the rotor reactor, and then, the temperature was cooled to 180 °C and kept steady. Subsequently, $^{13}\mathrm{CH_3}^{13}\mathrm{CH_2OH}$ was fed into the MAS NMR rotor reactor by the helium carrier gas with a weight hourly space velocity (WHSV) of 0.5 h $^{-1}$. Meanwhile, the $^{13}\mathrm{C}$ MAS NMR spectra were recorded using a one pulse sequence with a spinning rate of 4.3 kHz, a 2 s recycle delay, and a $\pi/4$ pulse width of 3.3 $\mu\mathrm{s}$. After the in situ CF $^{13}\mathrm{C}$ NMR experiments, the samples were transferred into a 4 mm rotor for the $^{13}\mathrm{C}$ CP/MAS NMR and 2D $^{13}\mathrm{C}-^{13}\mathrm{C}$ dipolar-based COmbined R2 Driven (CORD) spin diffusion NMR experiment. The experiments were recorded at room temperature with a spinning rate of 12 kHz and a recycle delay of 2 s. A contact time of 3 ms was used in the CP/MAS experiment, and a mixing time of 10 ms was used in the CORD experiment, respectively.

Prior to the preparation of the cyclopentadienyl cations on H-ZSM-5 zeolites with different Si/Al ratios, about 20 kPa of $^{13}\text{CH}_3$ $^{13}\text{CH}_2$ OH saturated vapor was adsorbed in the pretreated zeolites at RT. After reaction at 150 °C for 30 min, the temperature was cooled to RT. Subsequently, samples after reaction were transferred into a 4 mm NMR rotor in a nitrogen glovebox for $^{14}\text{H}-^{13}\text{C}$ CP/MAS NMR experiments. A 12 kHz spinning rate and a 2 s recycle delay were used in the sequence. All the chemical shifts of

 $^{13}\mathrm{C}$ NMR spectroscopy were referenced to adamantane with the upfield methine peak at 29.5 ppm. The temperature of the probe mentioned above was calibrated using potassium bromide (KBr) as a heat indicator, according to the change of the chemical shift from $^{79}\mathrm{Br}$ MAS NMR spectra under different temperatures. The $^{79}\mathrm{Br}$ chemical shifts are linearly related to temperature with a slope of -0.0249 ppm/K. 27 The chemical shift was set to 0.0 ppm at 293 K. Therefore, the real-time temperature ($T_{\rm real}$) of sample can be deduced by the following equation, where δ represents the chemical shift of KBr at the actual temperature.

$$T_{\text{real}} = 293 - \delta/0.0249$$

2.4. Theoretical Calculation. In the structure optimization of adsorbed ethanol and diethyl ether, the electron correlation effects were modeled using the generalized gradient approximation (GGA) proposed by Perdew, Burke, and Ernzerhof (PBE method). ²⁸ In order to describe the interactions between the adsorbed ethanol, diethyl ether, and zeolite framework accurately, the DFT-D method was used in the structure optimization. In addition, the cutoff energy for the planewave basis set was set to 500 eV. All the calculations were performed using the CASTEP code as implemented in the Material Studio 6.0 software. ²⁹ In the optimization structure, the Al_{12} –

 ${\rm O}_{24}({\rm H}){-}{\rm Si}_{12}$ intersection site, located in the intersection of the straight channel and the sinusoidal channel of zeolite H-ZSM-5, was adopted to represent the Brönsted acid site. Because this site is easily accessed by adsorbents and has a maximum reaction space.

2.5. Catalytic Testing. The H-ZSM-5 zeolites were pressed and sieved into 40–60 meshes before the catalytic testing. Ethanol-to-olefins conversion was carried out on a fixed-bed quartz tubular reactor under atmospheric pressure. Before the reaction, the pellets (100 mg) were purged at 500 °C under a nitrogen atmosphere for 30 min to remove the adsorbed water and purities, and then, the reactor was cooled to 350 °C. The ethanol (Beijing Balinwei Technology Co. Ltd., purity >99.9%) was fed by passing the helium carrier gas through an ethanol saturator maintained at 20 °C. The WHSV of ethanol was 2.0 h⁻¹. The effluent products from reactor were analyzed by online gas chromatography equipped with a PoraPLOT Q-HT capillary column and a FID detector.

3. RESULTS AND DISCUSSION

3.1. Textural Characterizations of the H-ZSM-5-x Zeolites. First, the textural characterizations of the zeolite used in this work were investigated thoroughly. As demonstrated by XRD patterns (Figure 1a) and SEM (Figure 1b-e), the synthesized catalysts have good crystallization and homogeneous morphology. Moreover, all the H-ZSM-5 zeolites with different Si/Al ratios have similar particle sizes and crystal morphologies; the crystal size of the prismatic zeolite is approximately 500 nm as shown in Figure 1b-e. The ²⁷Al MAS NMR spectra (Figure 2a) show the local structure information of the H-ZSM-5 zeolites, with the tetracoordinated framework aluminum (Al_{IV}) species as the main in H-ZSM-5-26 and H-ZSM-5-45, accompanied by a small amount of extra-framework six-coordinated aluminum (Al_{VI}) species due to the high alumina content, while the H-ZSM-5-150 and H-ZSM-5-351 have only framework Al_{IV} species. The Si/Al ratios of the synthesized samples calculated from ²⁹Si MAS NMR spectra are consistent with the results of XRF (Table 1). As shown in Figure 2b, the peak intensity at -103ppm increases with the Si/Al ratios increasing, which demonstrates the higher silanol content of the sample with a higher Si/Al ratio. The N₂ adsorption results of these sample are shown in Table 2. All the samples exhibit comparable specific surface area and pore volume.

Table 2. N₂ Adsorption Results and Acid Amounts of Samples with Different Si/Al Ratios

	S_{BET}^{a}	S_{Micro}^{b}	V_{Total}^{c}	$V_{\mathrm{Micro}}^{}}}}}$	B acid ^d
sample	$\left(m^2/g\right)$	$\left(m^2/g\right)$	$\left(\text{cm}^3/\text{g}\right)$	$\left(\text{cm}^3/\text{g}\right)$	(mmol/g)
H-ZSM-5-26	374	261	0.21	0.12	0.401
H-ZSM-5-45	390	234	0.21	0.11	0.338
H-ZSM-5-150	395	200	0.21	0.09	0.058
H-ZSM-5-351	375	194	0.21	0.09	0.045

"BET method. bt -plot method. c At P/P_0 = 0.975, d clculated from 1 H NMR spectra.

Since the catalyst surface acidity is primarily dependent on the Si/Al ratios, the synthesized H-ZSM-5-x zeolites were supposed to have a significant difference in acidity, especially the Brönsted acid, which usually refers to the bridge hydroxyl group (SiOHAl) in zeolite framework. The ¹H MAS NMR spectra presented in Figure 2c were used to quantify the concentration of the different acid sites. The deconvoluted curves fitted by Dmfit software were used to get more information about the acid sites of the H-ZSM-5-x zeolite, in

which $3.9~\rm ppm$ was assigned to the Brönsted acid site typically. The other signals at 1.7 and 2.0 ppm were assigned to the isolated silanol groups (Si-OH) and geminal or vicinal Si-OH groups, respectively, while 2.5 and 3.0 ppm may attribute to the Al-OH species. 30 The broad peak at 5.0 ppm can be assigned to a second Brönsted acid site having an additional electrostatic interaction with the zeolite framework.³² Furthermore, another broad peak at 4.7 ppm in samples with a high Si/Al ratio may be caused by the internal silanols, 30,31 as the 29Si MAS NMR spectra also exhibit high Si-OH content (H-ZSM-5-150 and H-ZSM-5-351). Clearly, the concentrations of the Brönsted acid reduce from 0.401 to 0.045 mmol/g as the Si/Al ratios increase(Table 2). Hence, the textural characterizations evidenced that the crystal morphology, specific surface area, and pore volume of synthesized H-ZSM-5 samples are comparable, except for the surface acidity.

3.2. Study of Ethanol Conversion Process by in Situ **ssNMR.** In order to investigate the ethanol conversion process, the H-ZSM-5-26 zeolite was selected as a representative typically. First, the in situ 13C MAS NMR experiment of ¹³CH₃¹³CH₂OH conversion under batch-like condition was conducted using a 4 mm HX probe. As shown in Figure 3a, multiple signals are presented. The chemical shifts at 60.5 and 65.0 ppm can be assigned to the methene carbon of adsorbed ethanol on H-ZSM-5-26 zeolite, while the peaks at 67.5 and 69.5 ppm can be assigned to the methene carbon of adsorbed diethyl ether (DEE). In addition, the 17.0 and 13.3 ppm are assigned to the corresponding methyl carbon of ethanol and DEE, respectively. These ascriptions are consistent with the reported works.²¹ The different structure configurations of the adsorbed ethanol are responsible for this phenomenon of ethanol according to the theoretical calculation (Figure 3b,c), which is denoted as end-on (60.5 ppm) and side-on (65.0 ppm) orientations analogously to the adsorption of methanol on zeolites. The side-on orientation of ethanol is more firmly adsorbed due to the stronger H-bonding and resulted in a higher chemical shift, whereas adsorbed DEE shows a single orientation due to the more symmetrical structure (Figure 3d). The higher chemical shift (69.5 ppm) may be caused by the activation of the adsorbed DEE at a higher temperature, which tends to be at the protonated state (Figure 3e), as the signals at 69.5 ppm can only be obtained when the temperature is above 145 °C. The chemical shifts at 20-40 ppm, which can be ascribed to the oligomerized olefins, were also obtained when the temperature was above 174 °C. Therefore, the formation of ethene in this stage can be proven and subsequently transformed to the long chain olefins through oligomerization reaction. Furthermore, the weak signals at 144-154 and 250 ppm, which are regarded as characteristic peaks of cyclopentenyl cations in the MTO process, were acquired in the ethanol conversion process. With the increase of reaction temperature, a clear evolution of the active intermediate species was presented. Ethanol with end-on orientation was gradually activated and converted to side-on orientation as the chemical shift increased from 61.8 to 65.0 ppm, along with diethyl ether species formation and activation. Whereafter, ethene could be formed when the temperature increased to 174 °C. Then, the oligomerized olefins and cyclopentenyl cations revealed the secondary reaction of the produced

The *in situ* ¹³C MAS NMR experiment of ¹³CH₃¹³CH₂OH conversion under continuous flow (CF) conditions was

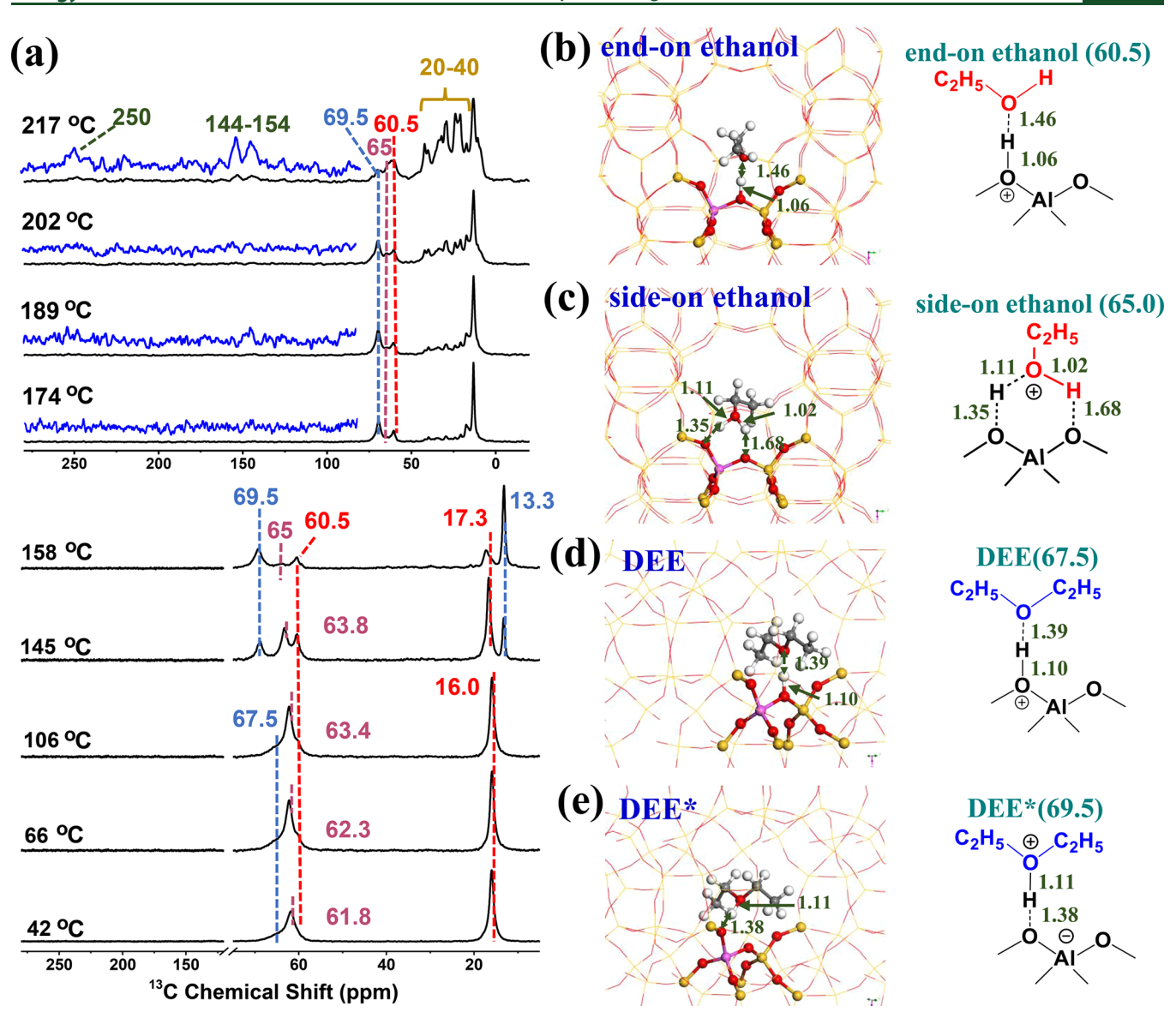


Figure 3. Temperature-programmed 13 C CP/MAS NMR spectra of 13 CH $_3$ ¹³CH $_2$ OH conversion on (a) H-ZSM-5-26 zeolite and (b–e) the structural configurations of surface adsorbed ethanol and DEE species. Color codes: O (red), Si (yellow), Al (pink), C (gray), H (white). The green numbers marked in b–e represent the distances between H and O atoms.

conducted to further monitor the exhaustive conversion process under real reaction conditions. Obviously, five peaks present on the spectra with reaction proceeding (Figure 4). In the first 10 min of the reaction, ethanol was adsorbed on H-ZSM-5-26 zeolite with a more stable side-on orientation and quickly dehydrated to diethyl ether, accompanied by the appearance of the peaks at 65.0 and 69.5 ppm. Only a chemical shift of 69.5 ppm for DEE was found under the reaction process, which corresponds to the activated state of DEE explained in Figure 3. The gradually decreased signal intensity of ethanol implies the conversion of the adsorbed ethanol. Conversely, the signal intensity of DEE presents an upward tendency, which means a dehydration process of ethanol to DEE. It is worthy to note that a weak peak at 85.0 ppm was observed after the reaction of 10 min, with the signal intensity growing up first and descending subsequently, since the oligomeric alkoxy species on acidic zeolites were supposed to have broad signals at 78.0 to 90.0 ppm in previous studies, 33,34 such as the trimethyloxonium ion (TMO) species, which was

reported in the methanol dehydration stage and showed a characteristic signal at 80.0 ppm. ³⁵ Therefore, the signal at 85.0 ppm may be assigned to the triethyloxonium ion (TEO) species in the dehydration stage of ethanol analogously. Zhou et al. also reported this species and emphasized its importance as an active intermediate in the formation of ethene from ethanol. ²¹ Therefore, the TEO active intermediate was also observed in the ethanol conversion process using *in situ* ¹³C MAS NMR.

In order to enhance the intensity and resolution of the signals of the sample after *in situ* reaction, the $^{1}H^{-13}C$ CP/MAS NMR experiment was conducted at room temperature (Figure 5a). The existence of a more pronounced peak at 85.0 ppm further confirmed the TEO species mentioned in Figure 4. Compared to the *in situ* ^{13}C MAS NMR spectra, the chemical shifts of the methene carbon of ethanol and DEE move to higher field from 65.0 to 60.5 and from 69.5 to 67.5 ppm, respectively, which implies that the temperature may have significant effects on the adsorbed ethanol and DEE. With

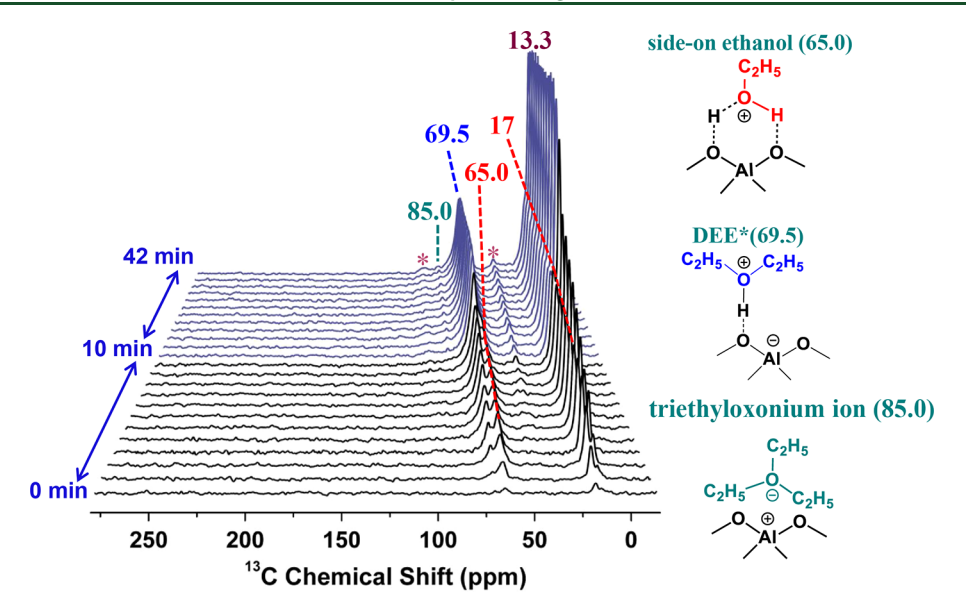


Figure 4. In situ CF 13 C MAS NMR for the observation of 13 CH $_2$ OH conversion over H-ZSM-5-26 zeolite under real-time conditions. The spectra were recorded at every 30 s from 0 to 10 min, then every 2 min from 10 to 30 min, and finally every 4 min from 30 to 42 min. The ethanol conversion was proceeded at 180 $^{\circ}$ C with a WHSV of 0.5 h $^{-1}$. Asterisks marked in the spectra were denoted the spinning sideband.

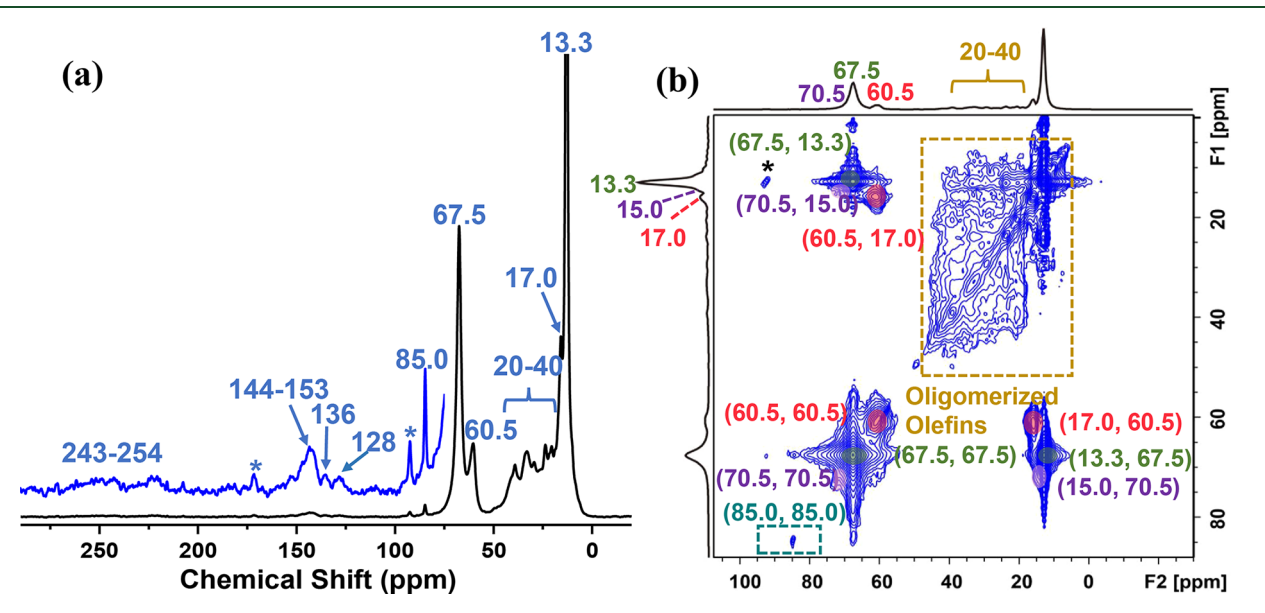


Figure 5. (a) ¹³C CP/MAS NMR spectrum and (b) 2D ¹³C-¹³C CORD MAS NMR spectrum of the sample after the *in situ* CF reaction of ethanol over H-ZSM-5-26. Asterisks marked in the spectra were denoted the spinning sideband. The spectra were recorded at room temperature.

the temperature cooling down, the adsorbed ethanol with the side-on orientation may return to the end-on orientation, which is consistent with the results mentioned in Figure 3, as the ethanol with end-on orientation mainly exists under a low temperature (42–106 °C). Meanwhile, the effect of temperature to activate the adsorbed DEE was also consolidated directly. Furthermore, the 13C NMR chemical shifts at approximately 128 and 136 ppm, assigned to aromatic moieties, were obtained. The weak signals at 144-153 and 243-254 ppm, which are regarded as characteristic peaks of cyclopentenyl cations, were also presented. Involved as active intermediates, cyclic carbocations and aromatics are emphasized as hydrocarbon-pool (HCP) species and form the supramolecular reaction centers with the inorganic zeolite framework in the MTO reaction to mediate the formation of olefins. 36,37 Especially cyclopentadienyl cations, are reported

have high activity in the formation of ethene and propene *via* a paring mechanism or cyclopentadienes-based cycle mechanism. Therefore, it can be speculated that cyclopentenyl cations captured in this work also have a significant role on ethanol conversion.

To gain more insights into the captured active species in ethanol conversion process, a two-dimensional $(2D)^{13}C-^{13}C$ CORD NMR spectrum was acquired and is shown in Figure 5b. A short mixing time of 10 ms was used to rule out the correlation between the intermolecular. An intense cross peak correlated a methyl resonance peak at 13.3 ppm with a $-CH_2O$ resonance peak at 67.5 ppm, which confirms the adsorbed DEE species. Similarly, the correlation of 17.0 and 60.5 ppm is assigned to ethanol. The existence of 85.0 ppm also confirmed the TEO species mentioned in Figure 4. In addition, a correlation of 70.5 and 15.0 ppm is observed and

assigned to methene carbon and methyl carbon of ethoxy species, respectively. The lack of this signal in *in situ* experiment may be caused by the overlap of the DEE signal at 69.5 ppm. The captured ethoxy emphasized its role as an initial active surface alkoxy species adsorbed on zeolite and thereafter mediated the formation of ethene. $^{19-21}$

In general, the kinds of active intermediate species were captured using multiple ssNMR experiments. In addition, a particular evolution process of these captured species can be summarized as the following: ethene was produced by the dehydration of ethanol *via* the DEE, ethoxy and TEO species; then, the produced ethene transformed to cyclopentenyl cations through oligomerization and cyclization, which is known as secondary reactions. This process has a high similarity to the methanol dehydration process, which indicated a strong potential that the captured cyclopentenyl cations have an analogical role in the formation of light olefins.

3.3. Role of the Captured Cyclopentenyl Cations in the Ethanol Conversion Process. H-ZSM-5 zeolites with different Si/Al ratios were used to further investigate the roles of captured cyclopentenyl cations in the ethanol conversion process. After the reaction of adsorbed ¹³CH₃¹³CH₂OH on H-ZSM-5- α zeolites at 150 °C for 1 h, the ¹³C CP/MAS spectra of these samples are presented in Figure 6. A distinct tendency

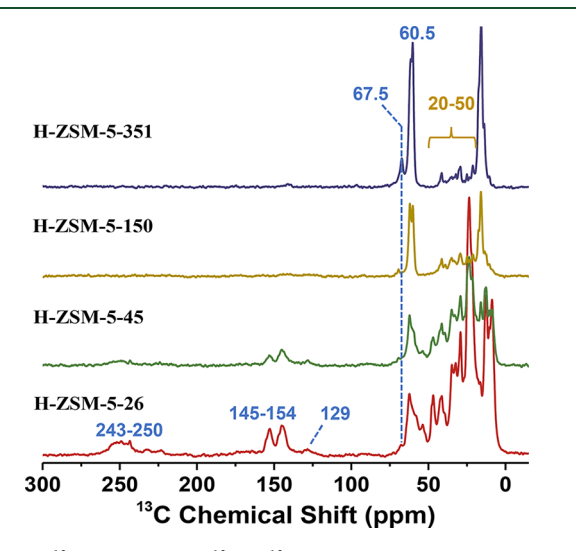


Figure 6. 13 C CP/MAS of 13 CH $_3$ 13 CH $_2$ OH conversion on H-ZSM-5 zeolites with different Si/Al ratios at 150 $^{\circ}$ C for 1 h.

is shown that the intensity of the signals corresponding to cyclopentenyl cations intermediates (145–154 ppm) declined with the Si/Al ratios of the used H-ZSM-5 zeolites increasing from 26 to 351. Meanwhile, the intensity of signals at 20–50 ppm also suffered a significant drop. Conversely, the adsorbed ethanol and DEE become more dominating on the H-ZSM-5-351 zeolite compared to the oligomerized olefins and cyclopentenyl cations. Therefore, it can be deduced that the concentration of the cyclopentenyl cations intermediates is positively associated with the Si/Al ratios, that is, the concentration of Brönsted acid sites of the H-ZSM-5 zeolite used. The more Brönsted acid sites would promote the secondary reactions such as oligomerization, cyclization, and aromatization in the ethanol conversion.

The catalytic performances of the H-ZSM-5-*x* zeolites were further studied in Figure 7 to elucidate the relationship between the obtained cyclopentenyl cations and the product

distribution. Compared to other catalysts, H-ZSM-5-351 shows a lower conversion of 85% and then quickly drops to 64%, which is primarily due to the lack of sufficient Brönsted acid sites for ethanol conversion. Furthermore, it is revealed that the Si/Al ratios of the H-ZSM-5 zeolite also have a significant effect on the selectivity of the light olefins like ethene and propene. H-ZSM-5-26 shows a comparable selectivity of ethene, propene, and C₄, which are 25.5%, 16.0%, and 26.6%, respectively (Figure 7a). While for other zeolites with higher Si/Al ratios (Figure 7b-d), the density of Brönsted acid sites decreases and ethene is the primary product with selectivity keeping above 97%, accompanied by a trace of propene and other products like C₄⁺. Moreover, acetaldehyde also appears in the effluent products for H-ZSM-5 zeolites with high Si/Al ratios, especially at the initial stage of the reaction. Its selectivity increases with the increase of Si/Al ratios. It is speculated that acetaldehyde may play a role in the early stage of ethanol conversion and is related to the acid sites of zeolites. The detailed mechanism of the formation of acetaldehyde is worthy of further study. In addition, the selectivity of the propene decreases sharply from 16.0% to 0.01% with the Si/Al ratios increase from 26 to 351.

Combined with the results of the Figure 6, deeper information can be dug that the catalyst that produced a higher concentration of cyclopentenyl cations intermediates also has a higher propene selectivity at 350 °C. However, H-ZSM-5-150 and H-ZSM-5-351, which almost have no cyclopentenyl cations signals, exhibited an ignorable propene yield; the dehydration of ethanol to ethene is the dominating reaction. It is mainly due to the lack of sufficient Brönsted acid sites for the secondary reactions of produced ethene such like oligomerization and cyclization. Serving as the hydrocarbon-pool (HCP) species, cyclopentenyl cations emphasized their importance in MTO reaction in massive amounts of research to mediate the formation of light olefins. 40,41 Similarly, these carbenium species may also exhibited their vital role in regulating the product distribution in ethanol conversion.

4. CONCLUSION

The conversion of ethanol over H-ZSM-5 zeolite was investigated specifically in this work with the assistance of multiple ssNMR technologies. Several active intermediates were captured in the conversion of ethanol like ethyl ether (DEE), ethoxy, triethyloxonium ion (TEO), and even cyclopentadienyl cations. Moreover, the adsorbed ethanol with different configurations referred to as side-on and end-on orientations were revealed in this work, which was analogous to the methanol adsorption behavior on zeolites in MTO reaction. The activated DEE was also observed in this work. Therefore, the evolution process of the captured intermediates can be concluded as the following: ethanol first undergoes a dehydration process to produce ethene via the DEE, ethoxy and TEO active intermediates, and then, the produced ethene transforms to cyclopentenyl cations through oligomerization and cyclization. Moreover, the concentration of cyclopentadienyl cations decreased with the decreasing of the Brönsted acid sites of H-ZSM-5 zeolites, which also contributed to a sharp downward trend on the selectivity of propene simultaneously. Hence, cyclopentadienyl cations were also supposed to have important effects in the ethanol conversion in this work and are closely correlated with the formation of propene products. In addition, these results will contribute to a better understanding of the mechanism of

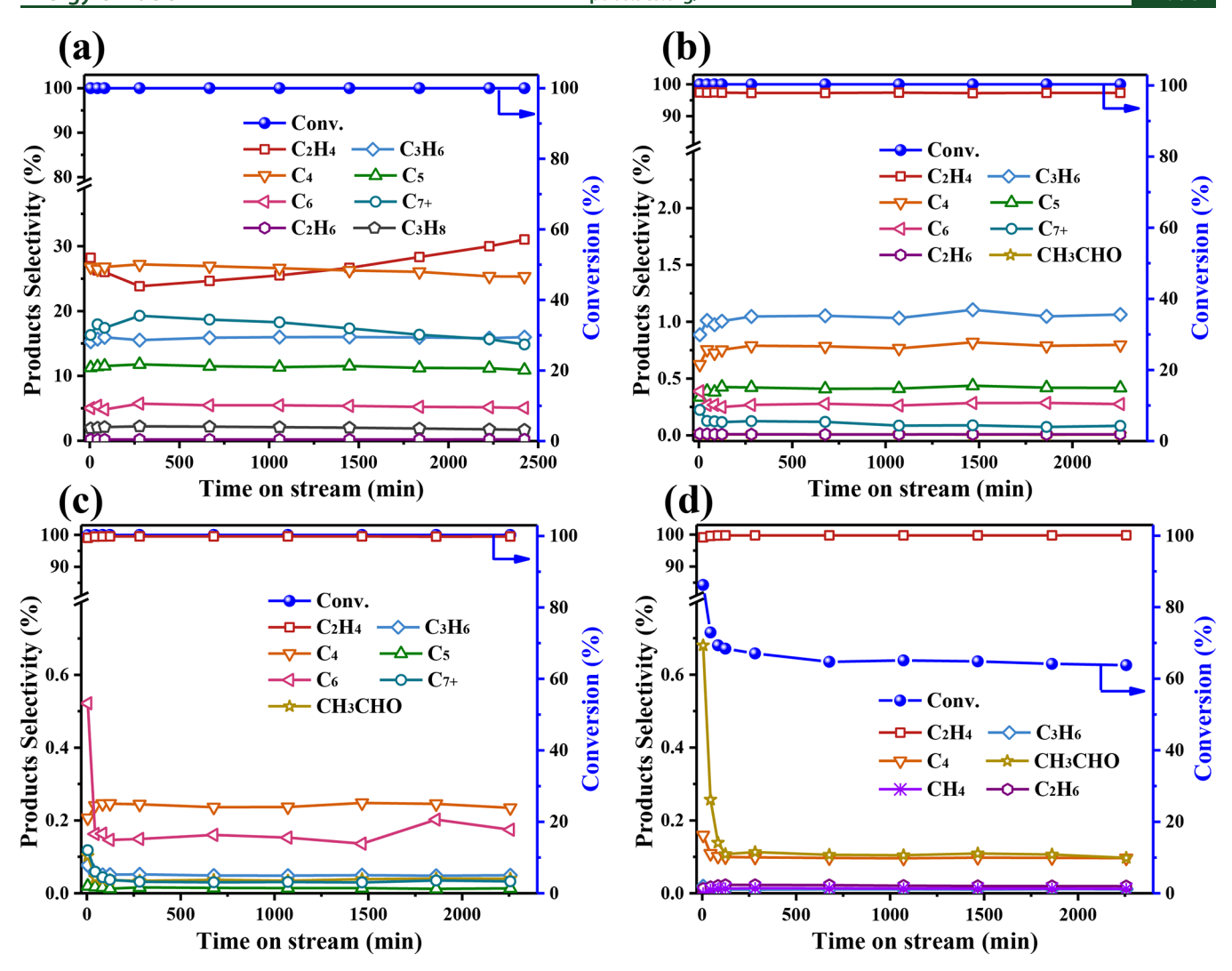


Figure 7. Conversion and products selectivity of ethanol conversion versus time on stream over samples with different Si/Al ratios at 350 °C: (a) H-ZSM-5-26, (b) H-ZSM-5-45, (c) H-ZSM-5-150, and (d) H-ZSM-5-351.

ethanol conversion to olefins and a guidance of improving the catalytic performance on the selectivity of propene.

AUTHOR INFORMATION

Corresponding Authors

Zhongmin Liu — National Engineering Laboratory for Methanol to Olefins, Dalian National Laboratory for Clean Energy, iChEM (Collaborative Innovation Center of Chemistry for Energy Materials), Dalian Institute of Chemical Physics, Chinese Academy of Sciences, Dalian 116023, P. R. China; University of Chinese Academy of Sciences, Beijing 100049, P. R. China; State Key Laboratory of Catalysis, Dalian Institute of Chemical Physics, Chinese Academy of Sciences, Dalian 116023, P. R. China; orcid.org/0000-0002-7999-2940; Email: liuzm@dicp.ac.cn

Shutao Xu — National Engineering Laboratory for Methanol to Olefins, Dalian National Laboratory for Clean Energy, iChEM (Collaborative Innovation Center of Chemistry for Energy Materials), Dalian Institute of Chemical Physics, Chinese Academy of Sciences, Dalian 116023, P. R. China; orcid.org/0000-0003-4722-8371; Email: xushutao@dicp.ac.cn

Authors

Shu Zeng — National Engineering Laboratory for Methanol to Olefins, Dalian National Laboratory for Clean Energy, iChEM (Collaborative Innovation Center of Chemistry for Energy Materials), Dalian Institute of Chemical Physics, Chinese Academy of Sciences, Dalian 116023, P. R. China; University of Chinese Academy of Sciences, Beijing 100049, P. R. China

Junjie Li – State Key Laboratory of Catalysis, Dalian Institute of Chemical Physics, Chinese Academy of Sciences, Dalian 116023, P. R. China

Nan Wang — National Engineering Laboratory for Methanol to Olefins, Dalian National Laboratory for Clean Energy, iChEM (Collaborative Innovation Center of Chemistry for Energy Materials), Dalian Institute of Chemical Physics, Chinese Academy of Sciences, Dalian 116023, P. R. China; University of Chinese Academy of Sciences, Beijing 100049, P. R. China

Wenna Zhang — National Engineering Laboratory for Methanol to Olefins, Dalian National Laboratory for Clean Energy, iChEM (Collaborative Innovation Center of Chemistry for Energy Materials), Dalian Institute of Chemical Physics, Chinese Academy of Sciences, Dalian 116023, P. R. China

Yingxu Wei — National Engineering Laboratory for Methanol to Olefins, Dalian National Laboratory for Clean Energy, iChEM (Collaborative Innovation Center of Chemistry for Energy Materials), Dalian Institute of Chemical Physics, Chinese Academy of Sciences, Dalian 116023, P. R. China

Complete contact information is available at: https://pubs.acs.org/10.1021/acs.energyfuels.1c02151

Notes

The authors declare no competing financial interest.

ACKNOWLEDGMENTS

This work was supported by the National Natural Science Foundation of China (22022202, 22002157, 21991090, 21991092, 21972142, 91745109), LiaoNing Revitalization Talents Program (XLYC1807227, XLYC1808014), the Youth Innovation Promotion Association of the Chinese Academy of Sciences (2014165), the Key Research Program of Frontier Sciences, Chinese Academy of Sciences (QYZDY-SSW-JSC024), and International Partnership Program of Chinese Academy of Sciences (121421KYSB20180007).

■ REFERENCES

- (1) Farrell, A. E.; Plevin, R. J.; Turner, B. T.; Jones, A. D.; O'Hare, M.; Kammen, D. M. Ethanol can contribute to energy and environmental goals. *Science* **2006**, *311*, 506–508.
- (2) Sanchez, O. J.; Cardona, C. A. Trends in biotechnological production of fuel ethanol from different feedstocks. *Bioresour. Technol.* **2008**, *99*, 5270–5295.
- (3) Kennes, D.; Abubackar, H. N.; Diaz, M.; Veiga, M. C.; Kennes, C. Bioethanol production from biomass: carbohydrate vs syngas fermentation. *J. Chem. Technol. Biotechnol.* **2016**, *91*, 304–317.
- (4) Yang, C.; Miao, Z.; Zhang, F.; Li, L.; Liu, Y.; Wang, A.; Zhang, T. Hydrogenolysis of methyl glycolate to ethanol over a Pt–Cu/SiO₂ single-atom alloy catalyst: a further step from cellulose to ethanol. *Green Chem.* **2018**, *20*, 2142–2150.
- (5) Song, H.; Wang, P.; Li, S.; Deng, W.; Li, Y.; Zhang, Q.; Wang, Y. Direct conversion of cellulose into ethanol catalysed by a combination of tungstic acid and zirconia-supported Pt nanoparticles. *Chem. Commun.* **2019**, *55*, 4303–4306.
- (6) Xu, S.; Zhi, Y.; Han, J.; Zhang, W.; Wu, X.; Sun, T.; Wei, Y.; Liu, Z. Advances in catalysis for Methanol-to-Olefins Conversion. *Adv. Catal.* 2017, 61, 37–122.
- (7) Tian, P.; Wei, Y.; Ye, M.; Liu, Z. Methanol to Olefins (MTO): From Fundamentals to Commercialization. *ACS Catal.* **2015**, *5*, 1922–1938.
- (8) Tret'yakov, V. F.; Makarfi, Y. I.; Tret'yakov, K. V.; Frantsuzova, N. A.; Talyshinskii, R. M. The catalytic conversion of bioethanol to hydrocarbon fuel: A review and study. *Catalysis in Industry* **2010**, 2, 402–420.
- (9) Shioyama, T. Alcohol dehydration employing a zinc aluminate catalyst. U.S. Patent 4,260,845, 1981.
- (10) Viswanadham, N.; Saxena, S. K.; Kumar, J.; Sreenivasulu, P.; Nandan, D. Catalytic performance of nano crystalline H-ZSM-5 in ethanol to gasoline (ETG) reaction. *Fuel* **2012**, *95*, 298–304.
- (11) Xin, H.; Li, X.; Fang, Y.; Yi, X.; Hu, W.; Chu, Y.; Zhang, F.; Zheng, A.; Zhang, H.; Li, X. Catalytic dehydration of ethanol over post-treated ZSM-5 zeolites. *J. Catal.* **2014**, *312*, 204–215.
- (12) Gayubo, A. G.; Alonso, A.; Valle, B.; Aguayo, A. T.; Olazar, M.; Bilbao, J. Hydrothermal stability of HZSM-5 catalysts modified with Ni for the transformation of bioethanol into hydrocarbons. *Fuel* **2010**, *89*, 3365–3372.
- (13) Van Mao, R. L.; Levesque, P.; McLaughlin, G.; Dao, L. H. Ethene from ethanol over zeolite catalysts. *Appl. Catal.* **1987**, 34, 163–179.

- (14) Gayubo, A. G.; Alonso, A.; Valle, B.; Aguayo, A. T.; Olazar, M.; Bilbao, J. Kinetic modelling for the transformation of bioethanol into olefins on a hydrothermally stable Ni–HZSM-5 catalyst considering the deactivation by coke. *Chem. Eng. J.* **2011**, *167*, 262–277.
- (15) Gayubo, A. G.; Tarrío, A. M.; Aguayo, A. T.; Olazar, M.; Bilbao, J. Kinetic Modelling of the transformation of aqueous ethanol into hydrocarbons on a HZSM-5 Zeolite. *Ind. Eng. Chem. Res.* **2001**, *40*, 3467–3474.
- (16) Takahashi, A.; Fujitani, T. Conversion of bioethanol to propene over ZSM-5 zeolites. *J. Jpn. Pet. Inst.* **2018**, *61*, 20–27.
- (17) Bi, J.; Guo, X.; Liu, M.; Wang, X. High effective dehydration of bio-ethanol into ethene over nanoscale HZSM-5 zeolite catalysts. *Catal. Today* **2010**, *149*, 143–147.
- (18) Sun, J.; Wang, Y. Recent advances in catalytic conversion of ethanol to chemicals. ACS Catal. 2014, 4, 1078–1090.
- (19) Kondo, J. N.; Ito, K.; Yoda, E.; Wakabayashi, F.; Domen, K. An ethoxy intermediate in ethanol dehydration on Brönsted acid sites in zeolite. *J. Phys. Chem. B* **2005**, *109*, 10969–10972.
- (20) Wang, W.; Jiao, J.; Jiang, Y. J.; Ray, S. S.; Hunger, M. Formation and decomposition of surface ethoxy species on acidic zeolite Y. *ChemPhysChem* **2005**, *6*, 1467–1469.
- (21) Zhou, X.; Wang, C.; Chu, Y.; Xu, J.; Wang, Q.; Qi, G.; Zhao, X.; Feng, N.; Deng, F. Observation of an oxonium ion intermediate in ethanol dehydration to ethene on zeolite. *Nat. Commun.* **2019**, *10*, 1961–1961.
- (22) Chowdhury, A. D.; Paioni, L. A.; Whiting, G. T.; Fu, D.; Baldus, M.; Weckhuysen, B. M. Unraveling the homologation reaction sequence of the zeolite catalyzed ethanol-to-hydrocarbons process. *Angew. Chem., Int. Ed.* **2019**, *58*, 3908–3912.
- (23) Li, J.; Liu, M.; Li, S.; Guo, X.; Song, C. Influence of diffusion and acid properties on methane and propane selectivity in Methanol-to-Olefins reaction. *Ind. Eng. Chem. Res.* **2019**, *58*, 1896–1905.
- (24) Gao, S.; Xu, S.; Wei, Y.; Qiao, Q.; Xu, Z.; Wu, X.; Zhang, M.; He, Y.; Xu, S.; Liu, Z. Insight into the deactivation mode of methanol-to-olefins conversion over SAPO-34: Coke, diffusion, and acidic site accessibility. *J. Catal.* **2018**, *367*, 306–314.
- (25) Li, G.; Foo, C.; Yi, X.; Chen, W.; Zhao, P.; Gao, P.; Yoskamtorn, T.; Xiao, Y.; Day, S.; Tang, C. C.; Hou, G.; Zheng, A.; Tsang, S. C. E. Induced Active Sites by Adsorbate in Zeotype Materials. J. Am. Chem. Soc. 2021, 143 (23), 8761–8771.
- (26) Zhou, H.; Yi, X.; Hui, Y.; Wang, L.; Chen, W.; Qin, Y.; Wang, M.; Ma, J.; Chu, X.; Wang, Y.; Hong, X.; Chen, Z.; Meng, X.; Wang, H.; Zhu, Q.; Song, L.; Zheng, A.; Xiao, F. Isolated boron in zeolite for oxidative dehydrogenation of propane. *Science* **2021**, *372*, 76–80.
- (27) Thurber, K. R.; Tycko, R. Measurement of sample temperatures under magic-angle spinning from the chemical shift and spin-lattice relaxation rate of ⁷⁹Br in KBr powder. *J. Magn. Reson.* **2009**, *196*, 84–87.
- (28) Perdew, J. P.; Burke, K.; Ernzerhof, M. Generalized Gradient Approximation Made Simple. *Phys. Rev. Lett.* **1996**, *77*, 3865–3868.
- (29) Materials Studio 6.0; Accelrys Inc.: San Diego, CA, 2012.
- (30) Hunger, M.; Ernst, S.; Steuernagel, S.; Weitkamp, J. High-field ¹H MAS NMR investigations of acidic and non-acidic hydroxyl groups in zeolites H-Beta, H-ZSM-5, H-ZSM-58 and H-MCM-22. *Microporous Mater.* **1996**, *6*, 349–353.
- (31) Hunger, M. Brönsted acid sites in zeolites characterized by multinuclear solid-state NMR spectroscopy. *Catal. Rev.: Sci. Eng.* **1997**, *39*, 345–393.
- (32) Zhang, W.; Ma, D.; Liu, X.; Liu, X.; Bao, X. Perfluorotributylamine as a probe molecule for distinguishing internal and external acidic sites in zeolites by high-resolution ¹H MAS NMR spectroscopy. *Chem. Commun.* **1999**, 1091–1092.
- (33) Stepanov, A. G.; Luzgin, M. V.; Romannikov, V. N.; Sidelnikov, V. N.; Paukshtis, E. A. The nature, structure, and composition of adsorbed hydrocarbon products of ambient temperature oligomerization of ethene on acidic zeolite H-ZSM-5. *J. Catal.* **1998**, *178*, 466–477.

- (34) Nguyen, T. M.; Le Van Mao, R. Conversion of ethanol in aqueous solution over ZSM-5 zeolites: Study of the reaction network. *Appl. Catal.* **1990**, *58*, 119–129.
- (35) Fridgen, T. D.; McMahon, T. B. The reaction of protonated dimethyl ether with dimethyl Ether: temperature and isotope effects on the methyl cation transfer reaction forming trimethyloxonium cation and methanol. J. Am. Chem. Soc. 2001, 123 (17), 3980–3985.
- (36) McCann, D. M.; Lesthaeghe, D.; Kletnieks, P. W.; Guenther, D. R.; Hayman, M. J.; Van Speybroeck, V.; Waroquier, M.; Haw, J. F. A complete catalytic cycle for supramolecular methanol-to-olefins conversion by linking theory with experiment. *Angew. Chem., Int. Ed.* **2008**, *47*, 5179–5182.
- (37) Wang, C.; Wang, Q.; Xu, J.; Qi, G.; Gao, P.; Wang, W.; Zou, Y.; Feng, N.; Liu, X.; Deng, F. Direct detection of supramolecular reaction centers in the Methanol-to-Olefins conversion over zeolite H-ZSM-5 by ¹³C-²⁷Al solid-state NMR spectroscopy. *Angew. Chem., Int. Ed.* **2016**, *55*, 2507–2511.
- (38) Zhang, W.; Zhi, Y.; Huang, J.; Wu, X.; Zeng, S.; Xu, S.; Zheng, A.; Wei, Y.; Liu, Z. Methanol to olefins reaction route based on methylcyclopentadienes as critical intermediates. *ACS Catal.* **2019**, *9*, 7373–7379.
- (39) Lesthaeghe, D.; Horré, A.; Waroquier, M.; Marin, G. B.; Van Speybroeck, V. Theoretical insights on methylbenzene side-chain growth in ZSM-5 zeolites for methanol-to-olefin conversion. *Chem. Eur. J.* **2009**, *15*, 10803–10808.
- (40) Haw, J. F.; Nicholas, J. B.; Song, W.; Deng, F.; Wang, Z.; Xu, T.; Heneghan, C. S. Roles for cyclopentenyl cations in the synthesis of hydrocarbons from methanol on zeolite catalyst HZSM-5. *J. Am. Chem. Soc.* **2000**, *122*, 4763–4775.
- (41) Zhang, W.; Zhang, M.; Xu, S.; Gao, S.; Wei, Y.; Liu, Z. Methylcyclopentenyl cations linking initial stage and highly efficient stage in Methanol-to-Hydrocarbon process. *ACS Catal.* **2020**, *10*, 4510–4516.